RSC Advances

PAPER

View Article Online
View Journal | View Issue

Cite this: *RSC Adv.*, 2019, **9**, 1428

Differences between the binding modes of enantiomers *S*/*R*-nicotine to acetylcholinesterase

Ji Yang,[ab] Yongkuan Chen,*[b] Zhihua Liu,[b] Liu Yang,[b] Jianguo Tang,[b] Mingming Miao,[b] Na Gan[a] and Hui Li *[a]

Nicotine causes neurotoxic effects because it quickly penetrates the blood–brain barrier after entering the human body. Acetylcholinesterase (AChE) is a key enzyme in the central and peripheral nervous system associated with neurotoxicity. In this study, a spectroscopic method and computer simulation were applied to explore the mode of interaction between AChE and enantiomers of nicotine (*S*/*R*-nicotine). Fluorescence spectroscopy showed that the quenching mechanism of endogenous fluorescence of AChE by *S*/*R*-nicotine was static, as confirmed by the time-resolved steady-state fluorescence. The binding strength of both nicotine to AChE was weak (S-AChE: K_a = 80.06 L mol^{-1}, R-AChE: K_a = 173.75 L mol^{-1}). The main driving forces of S-AChE system interaction process were van der Waals force and hydrogen bonding, whereas that of R-AChE system was electrostatic force. Computer simulations showed that there were other important forces involved. *S*/*R*-Nicotine had a major binding site on AChE, and molecular docking showed that they bound mainly to the cavities enclosed by the active sites (ES, PAS, OH, AACS, and AP) in the protein. UV-vis spectroscopy and 3D spectroscopy indicated that nicotine significantly affected the microenvironment of Trp amino acids in AChE. The CD spectra indicated that *S*-nicotine increased the α-helical structure of AChE, but the overall conformation did not change significantly. By contrast, *R*-nicotine significantly changed the secondary structure of AChE. 5,5′-Dithiobis-2-nitrobenzoic acid (DTNB) method indicated that S and R nicotine produced different degrees of inhibition on the catalytic activity of AChE. Both experimental methods and computer simulations showed that *R*-nicotine had a significantly higher effect on AChE than *S*-nicotine. This research comprehensively and systematically analyzed the mode of interaction between nicotine and AChE for neurotoxicity assessment.

Received 4th December 2018
Accepted 3rd January 2019

DOI: 10.1039/c8ra09963d

rsc.li/rsc-advances

1. Introduction

Nicotine (Fig. 1) is an alkaloid found in Solanaceae species and is an important component in tobacco.[1] Nicotine is optically active, with both left-handed and right-handed conformations, namely *S*/*R*-nicotine; *S*-nicotine exists in naturally.[2,3] When nicotine enters the body through smoking cigarettes, it quickly passes through the blood–brain barrier into the brain, acting on the nicotine acetylcholine receptor.[4,5] Although the neurotoxicity of nicotine is considerable, studies on the interaction between nicotine and proteins are rarely reported. Acetylcholinesterase (AChE) is mainly distributed in the nervous system, particularly the brain, and can rapidly catalyze the hydrolysis of the neurotransmitter acetylcholine, leading to the termination of nerve impulse transfer, thereby ensuring the normal physiological functions of the human body.[6,7] AChE is closely related to cell development and maturation, promotes neuronal development and nerve regeneration, and is one of the most important enzymes in the nervous system. Any active substance in the brain that affects the activity of the enzyme may cause neurotoxicity.[8–10] Wang *et al.*[11] analyzed the interaction between AChE and enantiomers (BDE-47 and BDE-209) and found that BDE-209 has significant neurotoxic effect to humans. Moreover, BDE-47 is more likely to bind to AChE than BED-209.

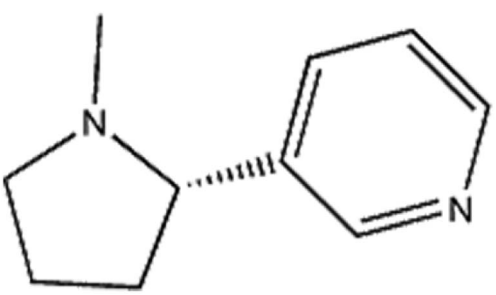

Fig. 1 The chemical structure of nicotine.

[a]*School of Chemical Engineering, Sichuan University, Chengdu, Sichuan, 610065, China. E-mail: lihuilab@sina.com; Fax: +86 028 85401207; Tel: +86 026 85405220*
[b]*R&D Center of China Tobacco Yunnan Industrial Co., Ltd., Kunming, 650231, China. E-mail: cyk1966@163.com*

Common methods used to investigate the binding of small ions or molecules to albumin proteins are fluorescence,[12,13] synchronous fluorescence,[14] UV-visible,[15,16] FTIR[17] and circular dichroism (CD)[18] spectroscopy, as well as equilibrium dialysis[19] and potentiometry.[20,21] Among these methods, equilibrium dialysis is used widely; but it requires the analysis of free and total drug concentration and takes a long time. In the potentiometric method, ion selective electrodes are used. Unfortunately, these electrodes are nonselective in case of many ligands, such as *e.g.* drug molecules.[20,21] Fluorescence spectroscopy is very helpful in protein–ligand interactions, because it can provide some useful information about the binding of ligands to protein such as binding mechanism, binding mode, binding constants and number of binding sites.[16]

Studying the interaction between *S*/*R*-nicotine and AChE has important significance for determining the damage mechanism and toxicology of nicotine in humans and also provides experimental and theoretical guidance for the development of new tobacco products. In this study, a variety of spectral methods were used to elucidate the binding mechanism of the AChE-*S*/*R*-nicotine systems, including binding strength, number of binding sites, thermodynamic constants, quenching mechanism, and other important parameters. Synchronous fluorescence spectroscopy and three-dimensional fluorescence spectroscopy combined with CD spectroscopy were used to explore the effect of *S*/*R*-nicotine on AChE structure. UV-vis spectroscopy was employed to validate the results. Comprehensive molecular docking and molecular dynamics (MD) simulations were applied to study the interaction mode under simulated physiological conditions. The theoretical prediction combined with the experimental results further confirmed the existence of a series of physical–chemical behaviors between the binary systems. The results help us understand the binding pattern between *S*/*R*-nicotine and AChE and assess the neurotoxicity of nicotine.

2. Reagents and methods

2.1 Reagents

AChE was purchased from Dalian Meilun Biotechnology Co., Ltd. (article number: MB0301); *S*-nicotine and *R*-nicotine were purchased from Mansite Biotech Co., Ltd. and Canadian TRC Chemical Co., Ltd.; 5,5′-disulfide (2-nitrophenylmethyl ester) (DTNB) and thioacetylcholine iodide (ATCh) were purchased from Tianjin Xiens Biochemical Technology Co., Ltd. The AChE mother liquor was dissolved in fresh Tris–HCl (pH 7.4) to a concentration of 0.5 mg L^{-1}, the nicotine mother liquor and the initial concentration at the time of purchase. All liquors were stored in a refrigerator at 277 K in the dark and diluted to desired concentration with Tris–HCl. All reagents were of analytical grade and triple distilled water was used throughout the experiment.

2.2 Methods

2.2.1 Steady-state fluorescence spectrum. Fluorescence spectra were measured in a Cary eclipse fluorescence spectrophotometer (Varian, CA, USA) equipped with a 1.0 cm quartz cell. The concentration of AChE was fixed at 0.075 mg L^{-1}, and the concentrations of *S*/*R*-nicotine were 0.124, 0.249, 0.373, 0.498, 0.622, and 0.746 mM. The excitation wavelength was set to 280 nm, and the emission wavelength in the range of 300–500 nm was detected. The excitation and emission slits were set to 20 and 10 nm, respectively. The maximum emission wavelength of 333 nm was chosen for further analytical calculations.

In the synchronous fluorescence spectroscopy, the excitation wavelength was 280 nm, the excitation and the emission slits were set to 20/10 nm, respectively, and the fluorescence emission spectra were scanned from 290 nm to 500 nm. The concentration of AChE was fixed at 0.075 mg L^{-1}. The concentrations of *S*/*R*-nicotine were 0.124, 0.249, 0.373, 0.498, 0.622, and 0.746 mM.

In the three-dimensional fluorescence spectroscopy, the photomultiplier tube voltage was 700 V, and the excitation and emission slits were both 10 nm. Scanning was performed at excitation wavelength range of 200–330 nm and emission wavelength range of 250–470 nm. The concentration of AChE was fixed at 0.075 mg L^{-1} and the concentration of *S*/*R*-nicotine was 0.746 mM.

2.2.2 Time-resolution fluorescence lifetime. The fluorescence lifetime of the sample solution was measured at room temperature using FluoroLog-3 (Horiba, France). The AChE concentration was fixed at 0.075 mg L^{-1}, the *S*/*R*-nicotine concentrations were 0.124 and 0.746 mM, and the fluorescence lifetime was determined after 30 min of reaction. The excitation wavelength was 280 nm and the emission wavelength was 345 nm.

2.2.3 UV-vis spectrophotometry. UV-vis spectrophotometer TU1901 was used to detect the presence and absence of *S*/*R*-nicotine. The concentration of AChE was fixed at 0.075 mg L^{-1}, and the concentrations of *S*/*R*-nicotine were 0.248, 0.373, and 0.622 mM. The detection wavelength range was 190–500 nm.

2.2.4 CD spectra. The CD spectrum of the sample solution was measured using Model 400 (Nova Biomedical, USA) at room temperature. The concentration of AChE was fixed at 0.075 mg L^{-1}, the concentrations of *S*/*R*-nicotine were 0.124 and 0.746 mM. The CD spectrum of each sample was determined after 30 min of reaction. The scanning wavelength was 180–260 nm, and the averages of three measurements were obtained.

2.2.5 Determination of AChE enzyme activity by DTNB method. For free AChE: 500 μL of 500 U L^{-1} AChE was added to 3 ml of Tris–HCl buffer solution (50 mM, pH 7.4), mixed, and incubated at 310 K for 20 min. Then 500 μL of 11 mM DTNB and 50 μL of 31 mM ATCh were added in sequence. The absorbance at 412 nm was measured every 30 s for 3 min.

For AChE in the presence of *S*/*R*-nicotine: 500 μL of 500 U L^{-1} AChE and 50 μL of 31 mM nicotine were added in 2.95 mL of Tris–HCl buffer solution (50 mM, pH = 7.4). The procedure for determination of free AChE was the same as described above.

2.2.6 Molecular docking. The binding pattern between all residues of AChE and *S*/*R*-nicotine was analyzed on the FlexX program[22] of the internal interface of LeadIT. The 3D structure

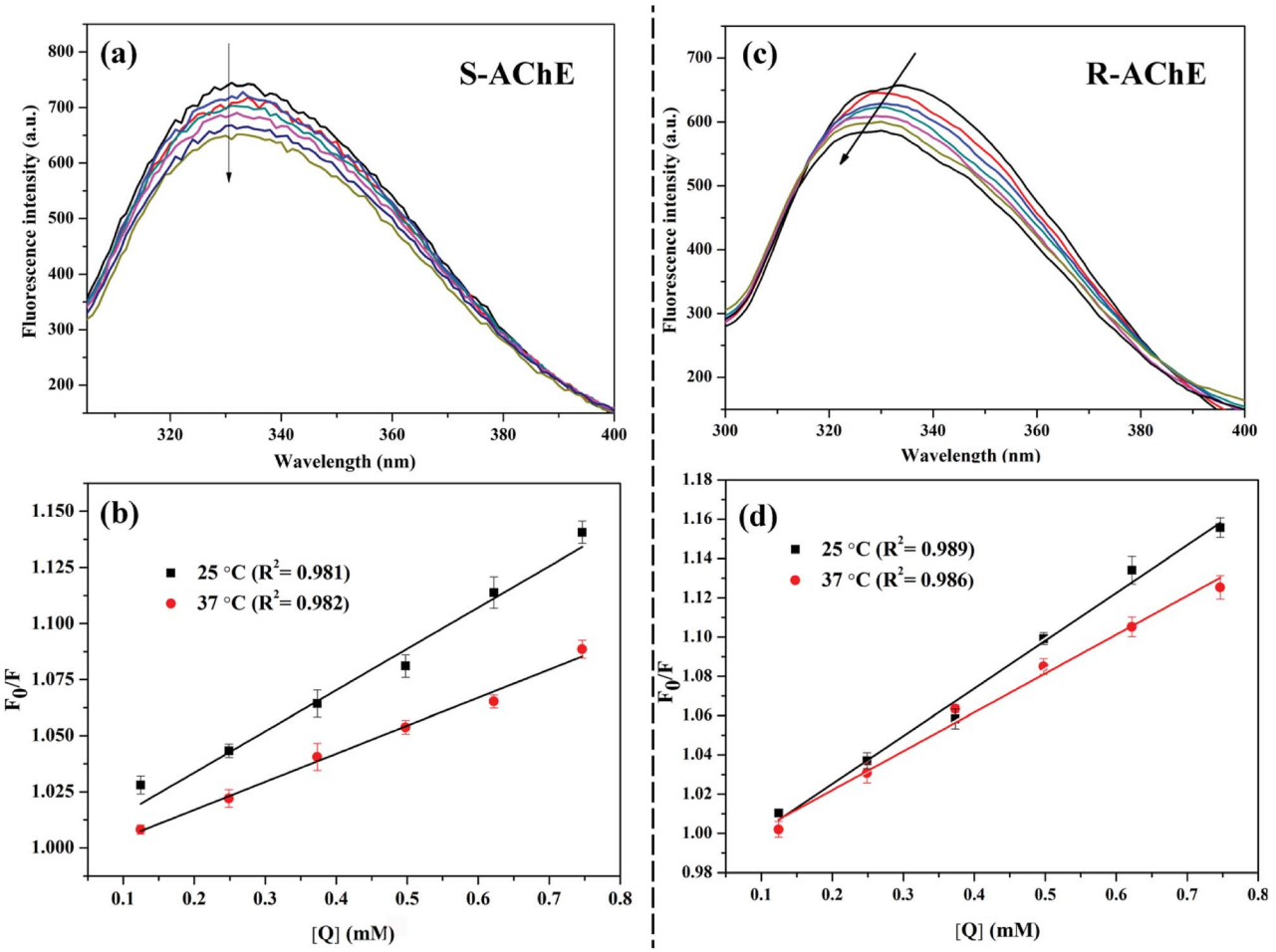

Fig. 2 Steady-state fluorescence spectra with increasing concentrations of AChE in the direction of the arrows; Stern–Volmer curves for fluorescence quenching at different temperatures. (a and b) AChE-*S*-nicotine system; (c and d) AChE-*R*-nicotine system.

of AChE was downloaded from the RCSB Protein Database (PDB code: 1qti). The foreign matter bound in the crystal structure was removed using the YASARA v17.4.17 (ref. 23) program, and the energy of the protein was optimized. The structure of nicotine was obtained from PubChem (PubChem CID: 89594 for *S*-nicotine, 157672 for *R*-nicotine). The correct tautomer and protonation state were specified, and the acceptor guide was used to add a hydrogen atom to the binding site residue. "Base fragment" was placed in the LeadIT (enthalpy and entropy driven ligand binding) using the FlexX hybrid algorithm. Other parameters were set at the default settings.

2.2.7 MD simulation. The MD simulation was carried out using YASARA v17.4.17. The molecular force field was selected by AMBER[24] force field.[14] The local charge number of each atom was calculated by AM1-BCC model.[25] The optimal conformation with the score first, and the free AChE were closed for further MD analysis. The simulation box was positioned large enough to accommodate all the atoms of the receptor protein, and periodic boundary conditions were applied. The pH was set to 7.4, the temperature was set to 298 K, and then sodium ions and chloride ions were randomly added to the system to keep them electrically neutral. The simulation results were performed using the MD macro (md run) preset in the YASARA software. The van der Waals force threshold was 8.0 Å, and the long-range electrostatic interaction was calculated using the Particle Mesh Ewald (PME) method. Multiple integration steps were used in the calculation: the intramolecular force was 1.25 fs and the intermolecular force was 2.5 fs; the trajectory was saved every 100 ps.

Table 1 Fluorescence decay fitting parameters of the AChE-nicotine system in the presence of different nicotine concentrations

System	C_{T6} (mM)	τ_1 (ns)	τ_2 (ns)	τ_3 (ns)	α_1	α_2	α_3	$\langle\tau\rangle$ (ns)	χ^2
AChE	0	2.295	0.532	5.669	0.428	0.110	0.462	3.659	1.088
AChE-S	0.4	2.423	0.539	5.811	0.452	0.121	0.427	3.641	1.119
	0.8	2.317	0.456	5.797	0.457	0.113	0.429	3.597	1.130
AChE-R	0.4	2.861	0.510	5.721	0.460	0.107	0.433	3.747	1.205
	0.8	2.209	0.471	5.598	0.472	0.112	0.416	3.524	1.179

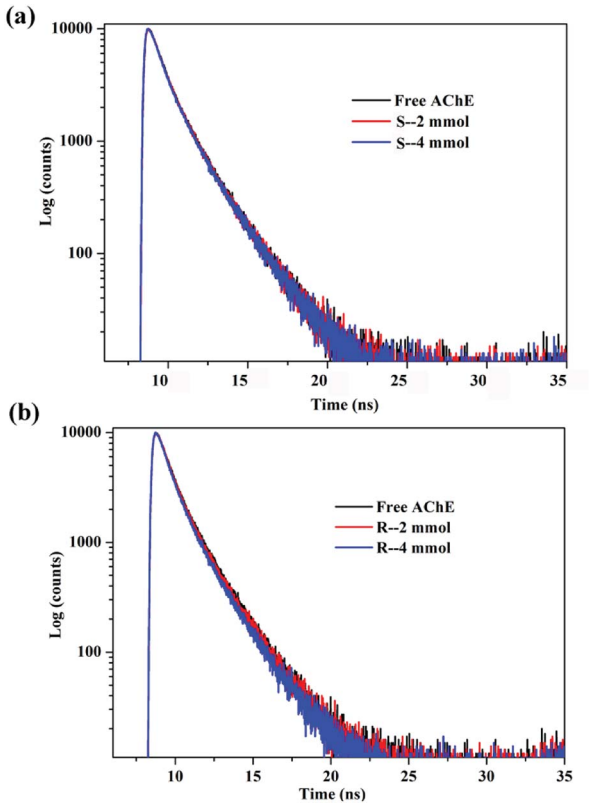

Fig. 3 Time-resolved fluorescence spectra of the system in a 298 K environment (a) AChE-*S*-nicotine (b) AChE-*R*-nicotine.

3. Results and discussion

3.1 Quenching mechanism research

AChE is a macromolecule protein with endogenous fluorescence. The fluorescence intensity of AChE decreases upon interaction with a small molecule; this phenomenon is called fluorescence quenching.[26] The quenching mechanism is divided into static and dynamic quenching, or a combination of two quenching mechanisms.[27] The most common way to determine the mechanism of quenching is by examining the dependence of the quenching constant on temperature and the change in the fluorescence lifetime of the protein in the presence of small molecules. As shown in Fig. 2(a and c), as the concentration of *S*/*R*-nicotine gradually increases, the fluorescence intensity of AChE gradually decreases. The quenching constant K_{sv} was calculated by using the Stern–Volmer equation:[28]

$$F_0/F = 1 + K_{sv}[Q] \quad (1)$$

where F_0 and F represent the fluorescence intensity of the free protein and the quencher–phosphor, [Q] represents the concentration of the quencher molecule, and K_{sv} is the quenching constant of the quencher–phosphor. Fig. 2(b and d) show that the K_{sv} values of both configurations of nicotine decreased with increasing temperature (Table 2), which was consistent with the static quenching mechanism.

To verify this result, we examined the fluorescence lifetime of AChE with different *S*/*R*-nicotine concentrations. The average life $\langle\tau\rangle$ was calculated by the following formula:[29]

$$\langle\tau\rangle = \alpha_1\tau_1 + \alpha_2\tau_2 + \alpha_3\tau_3 \quad (2)$$

The results are summarized in Table 1. The fitting results were evaluated with χ^2, and after three fittings, $\chi^2 \approx 1$, indicating that the fitting results were credible. The fluorescence lifetime map did not change significantly after adding different concentrations of *S*/*R*-nicotine (Fig. 3). The fluorescence lifetime of free AChE was approximately 3.659 ns. The addition of *S*-nicotine and *R*-nicotine caused the fluorescence lifetime of the protein to fluctuate at around 3.659 ns. However, the magnitude of the float was small, which may be caused by instrumental errors and differences in sample preparation. The results of fluorescence lifetime mapping were consistent with those obtained by the Stern–Volmer equation. Thus, the quenching mechanism of nicotine on the endogenous fluorescence of AChE was static quenching, and a ground-state complex is formed between the two molecules.[30]

3.2 Analysis of binding stoichiometry, strength, and stability

The binding strength of ligand to protein can be judged by the binding constant between two molecules. Given that AChE and nicotine undergo static quenching, the modified Stern–Volmer was used to calculate the binding stoichiometry (n) and binding constants (K_a):[31]

$$\log (F_0 - F)/F = \log K_a + n \log[Q] \quad (3)$$

where n is the number of binding sites and K_a is the binding constant. The value of n was deduced from the fluorescence experiment results (Table 2). *S*/*R*-Nicotine had only one major binding site on the AChE, and the results of the molecular docking further confirmed this finding. There are specific active sites on the AChE molecule: esteratic site (ES) consisting of

Table 2 Stern–Volmer quenching constants, binding parameters, and thermodynamic parameters of the AChE-nicotine system at different temperatures

System	T/K	K_{sv} (L mol^{-1})	K_a (L mol^{-1})	n	ΔG (kJ mol^{-1})	ΔH (kJ mol^{-1})	ΔS (J mol^{-1}K^{-1})
S-AChE	298	183.96 ± 5.21	80.06 ± 5.00	0.90 ± 0.11	−15.18	−82.62	−232.80
	310	107.65 ± 1.22	22.63 ± 4.35	0.74 ± 0.04	−15.45		
R-AChE	298	242.11 ± 10.10	173.75 ± 2.44	0.99 ± 0.04	−15.76	−12.19	11.17
	310	170.76 ± 5.34	144.65 ± 1.89	0.90 ± 0.07	−16.02		

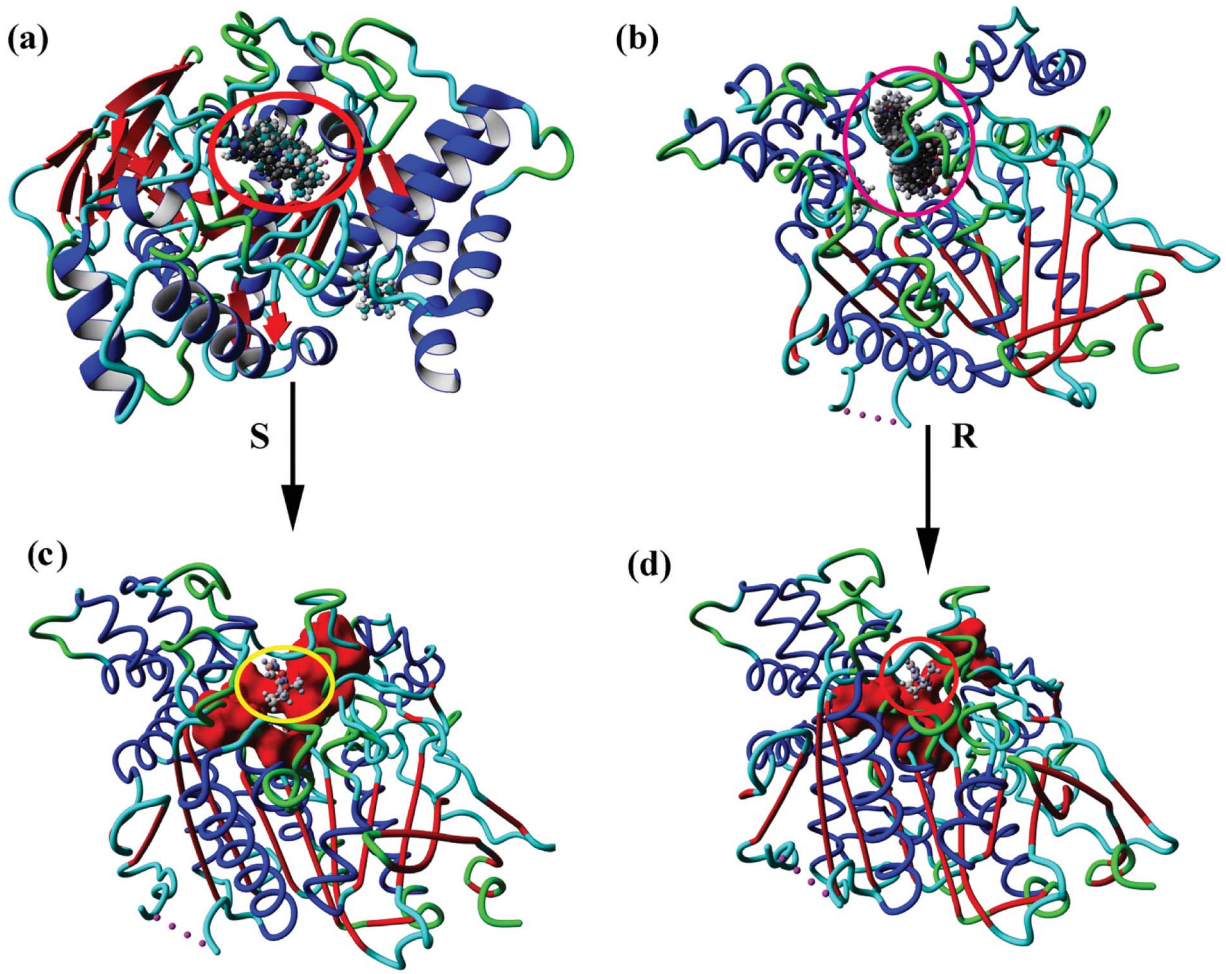

Fig. 4 Molecular docking of all 100 conformational maps for (a) AChE-*S*-nicotine and (b) AChE-*R*-nicotine. Optimal conformation of (c) AChE-*S*-nicotine and (d) AChE-*R*-nicotine.

Ser200, His440, and Glu327 (*i.e.*, catalytic triad); peripheral anionic site (PAS) consisting of some negatively charged Tyr (70, 121, 279) and Asp72; oxyanion hole (OH) consisting of Gly118, Gly119, Ala201, *etc.*; active site-selective aromatic binding sites (AACS) near the PAS and ES; and acyl pocket (AP) composed of Phe288 and Phe290.[32–34]

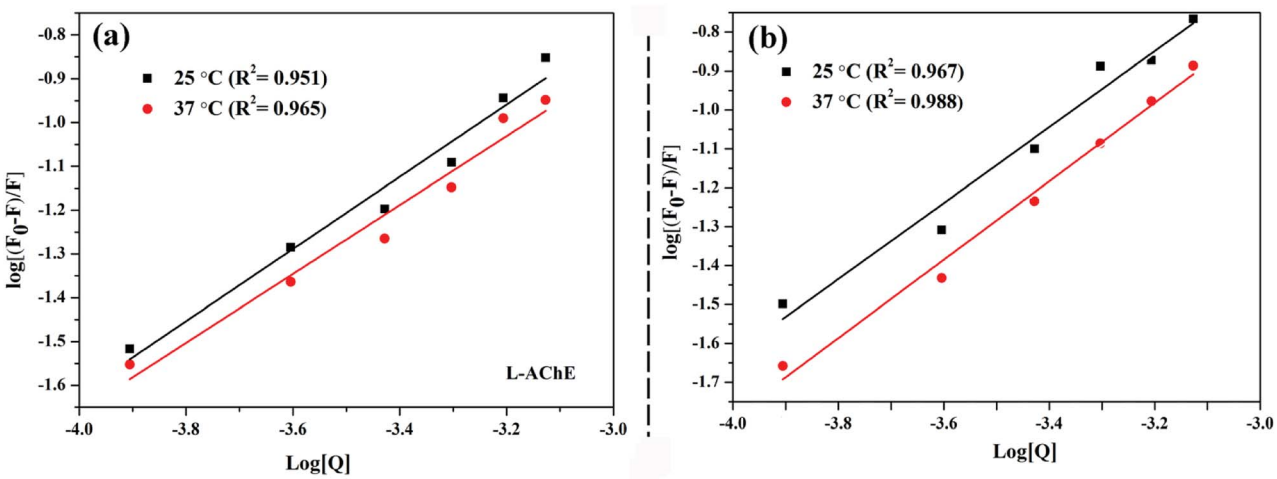

Fig. 5 Double logarithmic plot of fluorescence quenching at different temperatures: (a) AChE-*S*-nicotine system and (b) AChE-*R*-nicotine system.

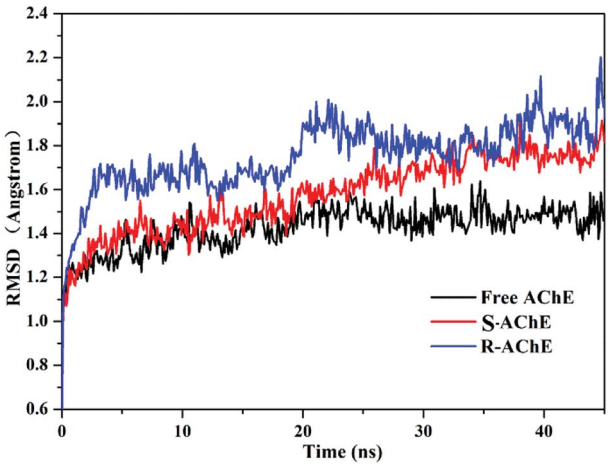

Fig. 6 Root mean square deviation (RMSD) of the skeleton Cα atom over time in the three systems.

Fig. 4(a and b) show the 100 conformations of the molecular docking results, which indicated the formation of clusters mainly at the same sites on the protein. Cluster analysis of all conformations yielded four major conformations for both *S*- and *R*-nicotine, and the first ones were combined in an active pocket surrounded by specific active sites as described above. Small molecules bind to the active site attachments and may interact with the amino acids that make up the active site, which in turn affects the related functional activities of proteins [Fig. 4(c and d)].

Fig. 5(a and b) showed that as the temperature increased, the binding constant between the two configurations of nicotine and protein decreased slightly (Table 2). The binding strength of R-AChE system was about an order of magnitude stronger than that of the S-AChE system, indicating that *R*-nicotine bound to AChE more strongly, but both systems were weakly bound.[1]

To investigate the binding stability, we selected the conformation scored first in the molecular docking to perform MD analysis. Fig. 6 shows the time-dependent root mean square deviation (RMSD)[36] of the three systems. The average order of the RMSD values of the three systems was R-AChE > S-AChE > free AChE, indicating that nicotine had a negative effect on the stability of the protein backbone. In addition, in the R-AChE complex system, the numerical fluctuation of RMSD was very obviously, this proved that *R*-nicotine induced the deviation of the protein skeleton of AChE seriously from the original position. Compared with *R*-nicotine, although *S*-nicotine increased the RMSD value of AChE, it generally showed a stable state, and the system tends to balance at around 35 ns.

The radius of gyration value (R_g)[37] of the three systems is shown in Fig. 7(a). The values of free AChE and S-AChE differed greatly at the initial phase, but they remained stable and started to overlap together at approximately 20 ns. Thus, *S*-nicotine did not affect the looseness of the AChE protein structure. The R_g value of R-AChE system deviated from the initial by about 0.4 angstrom, and the fluctuations were significant in the whole process, which suggested that *R*-nicotine made the structure of AChE looser and more unstable.

Comparison of the root mean square fluctuations (RMSF)[27] of the three systems [Fig. 7(b)] indicated that the coincidence degree between the free AChE and the S-AChE system was higher than that of AChE and R-AChE. In the latter system, the RMSF value of the residues with amino acid numbers 310–330 were significantly lower than that of free protein, which may be due to the hydrogen bonding (will be discussed later) between *R*-nicotine and protein during the simulation to make the conformation more mechanically stable.

3.3 Interaction force analysis

The following two formulas were used to obtain the thermodynamic constants and estimate the main interaction forces in the system:[38]

$$\ln K_a = -\Delta H/RT + \Delta S/R \quad (4)$$

$$\Delta G = \Delta H - T\Delta S \quad (5)$$

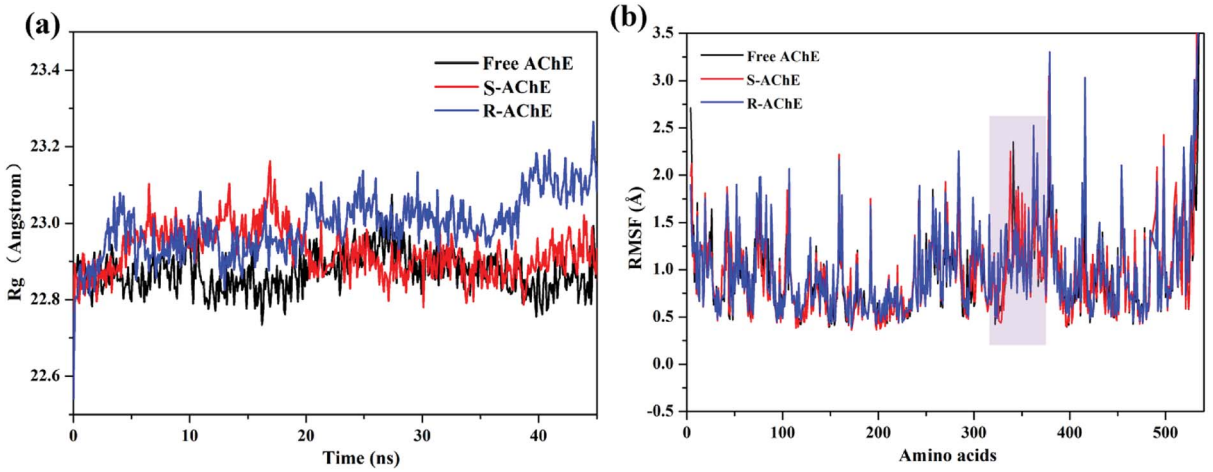

Fig. 7 (a) R_g and (b) RMSF values of three systems during MD calculation.

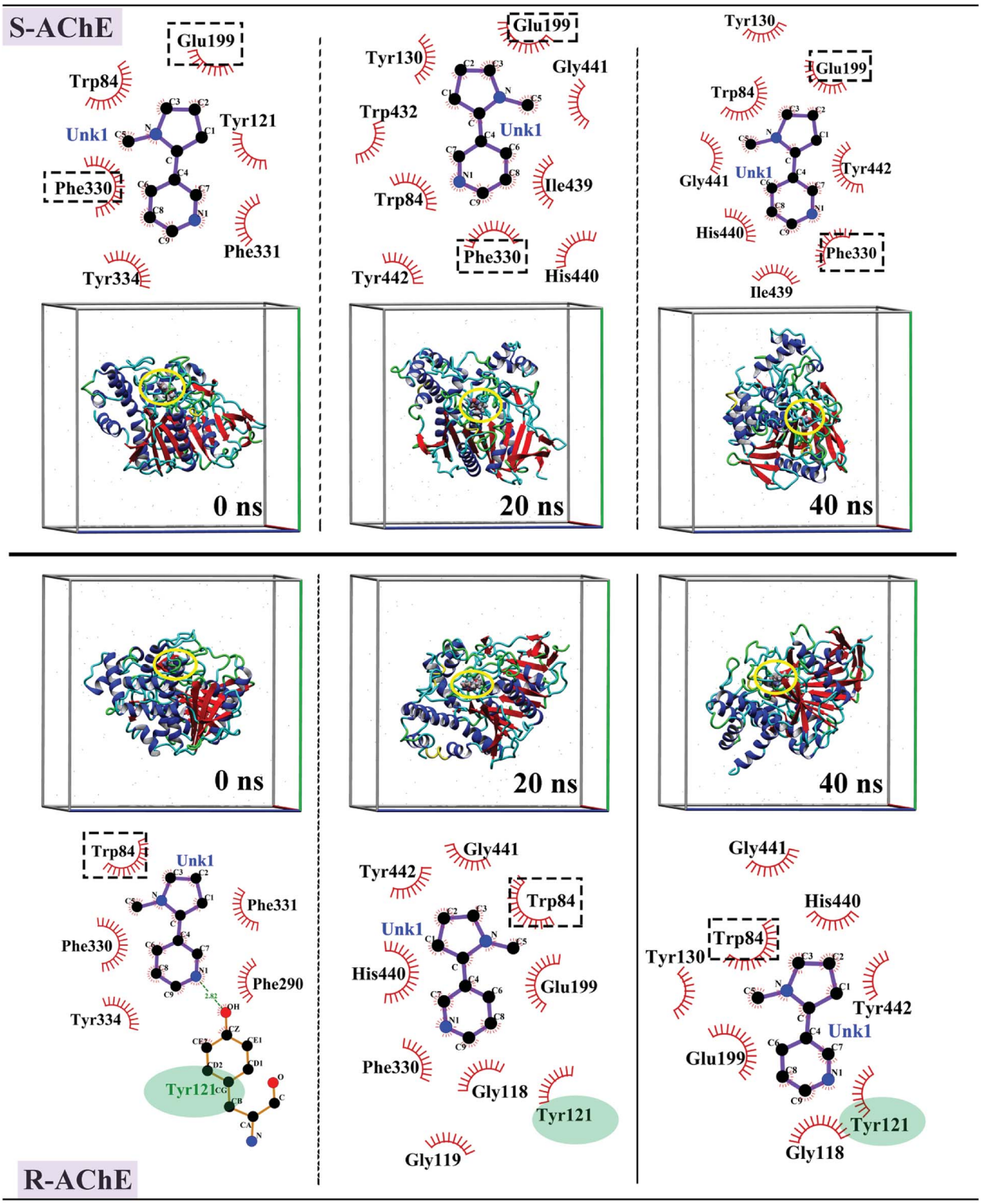

Fig. 8 Interaction force map and three-dimensional conformation of S-AChE complex (top) and R-AChE complex (bottom) of optimal conformation in MD simulation process.

where K_a is the binding constant at the corresponding temperature and R is the ideal gas constant (8.314 J mol^{-1} K^{-1}). The calculation results are summarized in Table 2. The experimental results showed that for the S-AChE system, the negative enthalpy change (ΔH) and the negative entropy (ΔS) change indicated that the main forces were van der Waals force and hydrogen bond. For the R-AChE system, the negative enthalpy change and the positive entropy change suggested that

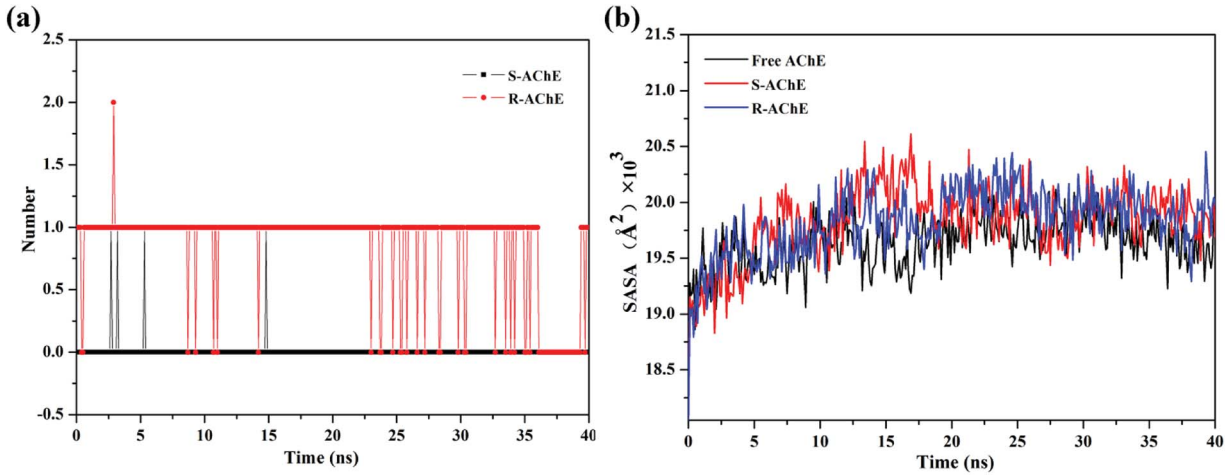

Fig. 9 (a) Number of hydrogen bonds in the simulation process and (b) SASA values in the simulation process.

electrostatic force played an important role in the binding process. In addition, the negative Gibbs free energy change (ΔG) reflected the spontaneity of the interaction process.[39–41]

The interaction forces were further analyzed using the simulation trajectory of different stages in the MD simulation process. As shown in the upper panel of Fig. 8, in the S-AChE system, *S*-nicotine has hydrophobic interaction with Trp84, Tyr121, Phe331, Phe330, Tyr334, and Glu199 amino acids near the binding site at 0 ns. Over time, the interaction between *S*-nicotine and surrounding amino acids changed, but Glu199, Phe330, and Trp84 interacted with *S*-nicotine throughout the process. The amino acid residues that participated in the second half of the simulation remained essentially unchanged. Thus, *S*-nicotine maintained a constant interaction with surrounding amino acid residues within the binding site, thereby maintaining the conformation in a relatively stable state.

The force interactions in R-AChE system presented a different situation. As shown in the lower panel of Fig. 8, at 0 ns, *R*-nicotine formed a hydrophobic interaction with Trp84, Phe331, PhE290, Tyr334, and Phe330, and there was a hydrogen bond of 2.82 Å between the hydrogen atom in the hydroxyl group of Tyr121 and the N atom in the nicotine molecule. Tyr121 and Trp84 interacted with *R*-nicotine in the entire simulation process. Tyr121 amino acid is an important component of the active site of the PAS and has a negative charge.

This observation was consistent with the conclusion that the R-AChE binding process was dominated by electrostatic interaction in the experiment. Moreover, Glu199 and His440 interacted with AChE in the latter half of the simulation, and these two amino acids are important constituent amino acids of OH and ES. Therefore, the binding of *R*-nicotine at this site may have a certain effect on the enzymatic hydrolysis function of AChE, which agreed with the experimental results of the enzyme activity test. Moreover, the simulated three-dimensional map showed that *S*/*R*-nicotine reversed the spatial conformation of AChE and changed the secondary structure.

The number of hydrogen bonds between small molecules and proteins is shown in Fig. 9(a). There was almost no hydrogen bond involved in the S-AChE system. However, according to the fluorescence experiment, we cannot rule out the existence of hydrogen bonding in the system. The reason for this discrepancy may be due to the limitations of computer algorithms, and it is impossible to simulate accurately the actual interactions. The experiment and computer simulation complement each other and can more fully analyze the forces

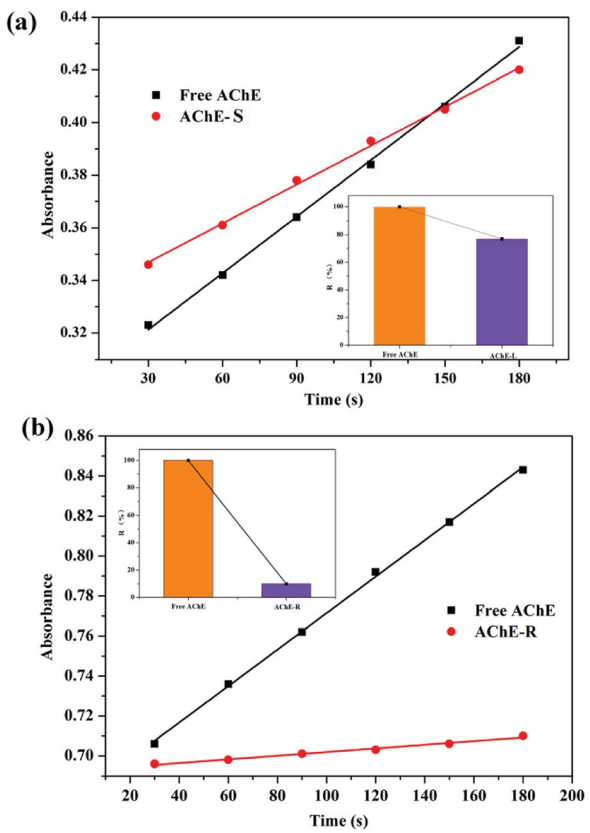

Fig. 10 Determination of enzyme catalytic activity of the (a) AChE-*S*-nicotine and (b) AChE-*R*-nicotine systems at 298 K.

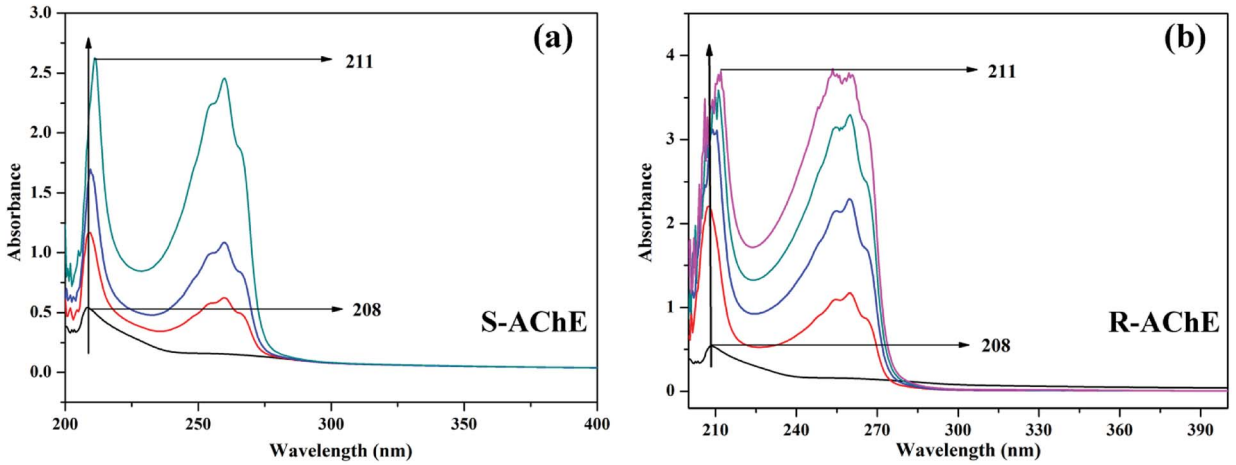

Fig. 11 UV-vis spectra of the (a) AChE-*S*-nicotine and (b) AChE-*R*-nicotine systems at 298 K. The concentration of the T6 in the direction of the arrow gradually increases.

that exist in the system. Hydrogen bond plays an important role in the R-AChE system. The above results showed that the interaction between small molecules and proteins is very complicated, and multiple binding forces may exist between the molecules owing to the huge molecular network of proteins.

The variation in solvent accessible surface area (SASA)[37] of the system was also analyzed, as shown in Fig. 9(b). The SASA values of both complex systems were increased slightly, indicating that AChE will be more exposed to the solvent than the free one, thus prompting the quencher (*S*/*R*-nicotine) to better contact the AChE and then quench the protein. The results further demonstrated that the *S*/*R*-nicotine interacted with AChE and affected the spatial conformation of amino acids.

3.4 Effect of *S*/*R*-nicotine on AChE enzyme activity

5,5′-Dithiobis-2-nitrobenzoic acid (DTNB) spectrophotometry is a sensitive method for detecting AChE activity.[42–45] Ultraviolet

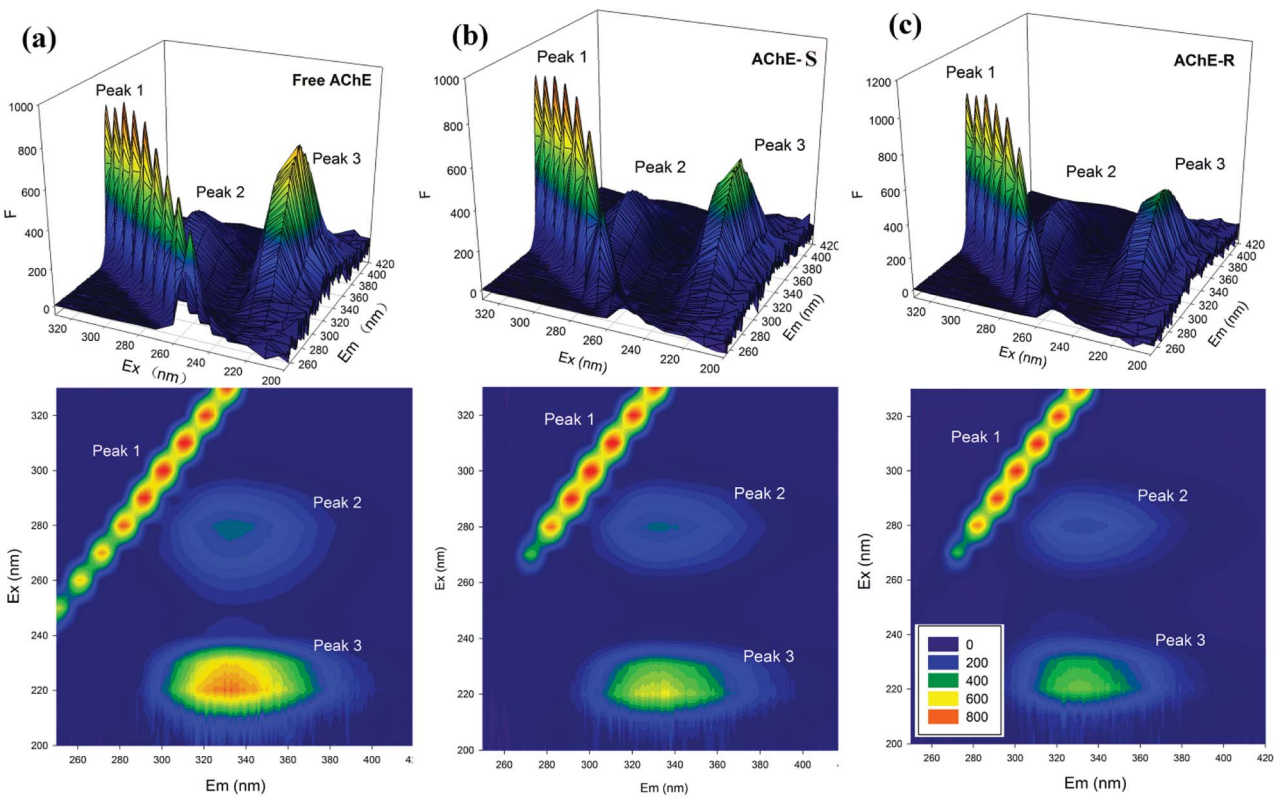

Fig. 12 3D fluorescence spectra of the (a) free AChE (b) AChE-*S*-nicotine and (c) AChE-*R*-nicotine systems in a 298 K environment (top: 3D map; lower: 2D map).

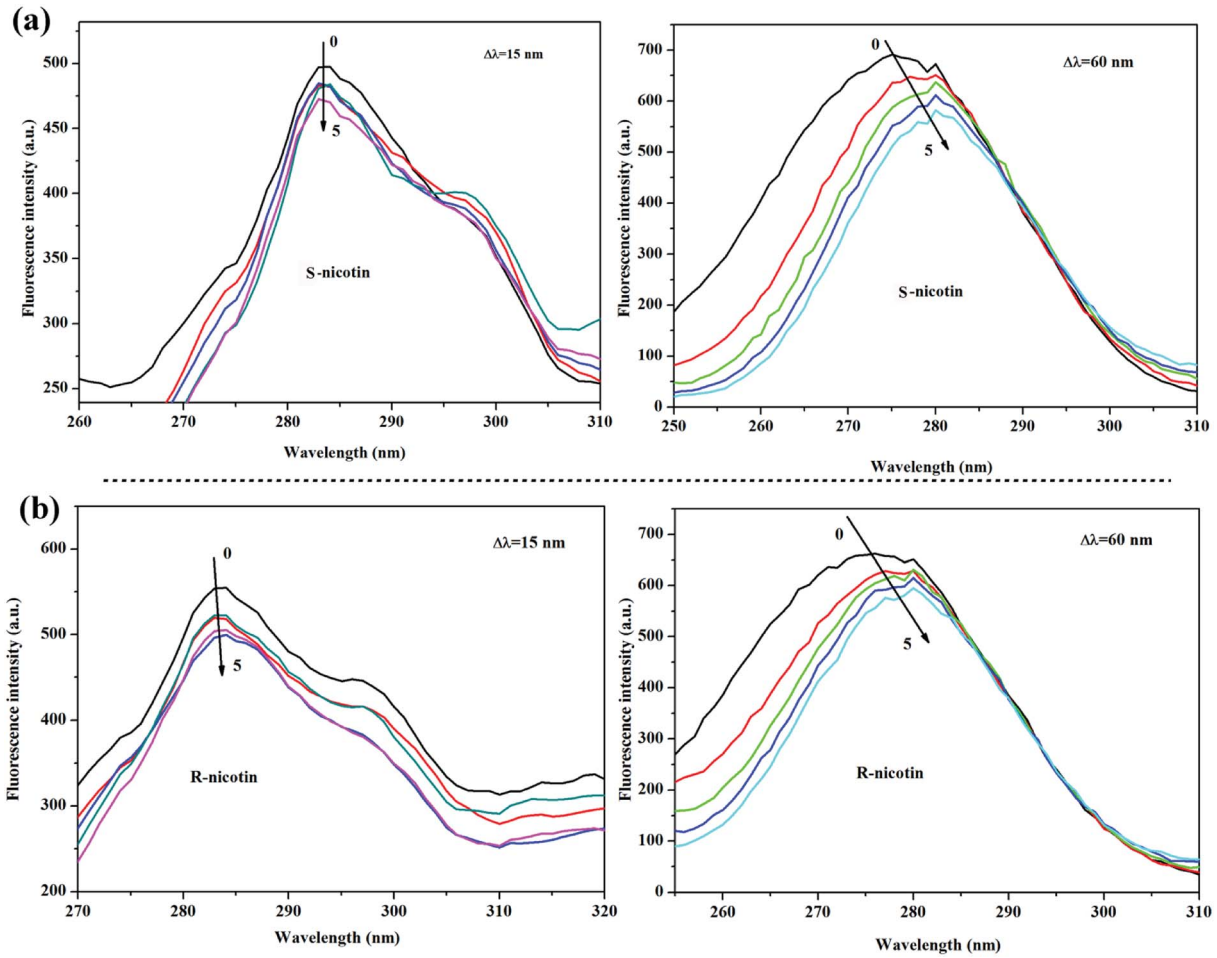

Fig. 13 Synchronous fluorescence spectra of the (a) AChE-*S*-nicotine and (b) AChE-*R*-nicotine systems at 298 K.

spectroscopy was used to detect the rate of catalytic production, and the effects of two configurations of nicotine on the enzymatic activity of AChE were qualitatively investigated. Both *S*- and *R*-nicotine reduced the catalytic activity of AChE (Fig. 10), but the latter's effect intensity was significantly greater than the former. According to the results of MD simulation, this phenomenon may be closely related to the Trp121 amino acid near the *R*-nicotine binding site, based on the hydrogen bond and hydrophobic interaction between the two molecules. Combined with the results of UV-vis spectroscopy and CD spectroscopy, *R*-nicotine had a greater effect on the structure and amino acid microenvironment of AChE than *S*-nicotine, and it had a greater degree of inhibition on the catalytic function of AChE.

3.5 Effect of nicotine on AChE conformation

3.5.1 UV-vis absorption spectroscopy. UV-vis absorption spectroscopy is a commonly used method to study the interaction between drugs and proteins. When the drug and protein combine, the chromophore absorption peak position or peak width of the biomacromolecular protein may be changed, which can be used to determine the influence of the binding on the protein conformation.[46] As shown in Fig. 11, the absorption spectrum of AChE at around 205 nm corresponds to the peptide bond absorption of the AChE.

When *S*- or *R*-nicotine combines with AChE, the absorption spectrum of AChE changed; not only its maximum absorption intensity was significantly enhanced, but also the peak position of its maximum absorption wavelength was redshifted. This phenomenon indicated that *S*/*R*-nicotine changed the microenvironment of AChE amino acid residues, causing a change in AChE conformation.

3.5.2 Three-dimensional (3D) fluorescence spectroscopy. As a mature and perfect analytical method for studying the conformational changes of proteins, 3D fluorescence spectroscopy has been favored by researchers in recent years. It provides more complete and reliable spectral information than conventional fluorescence spectroscopy.[47] The 3D spectrum includes 3D projections and contour maps. In Fig. 12, peak 1 is a Rayleigh scattering peak, $\lambda_{ex} = \lambda_{em}$, peak 2 mainly reflects the fluorescent characteristic of the tryptophan residue, and peak 3 reflects the characteristic of the polypeptide main chain structure.[48] The same concentration of *S*- and *R*-nicotine produced different degrees of influence on AChE. The nicotine of both configurations changed the contour density of the AChE 3D spectrum, and the intensity decreased significantly. However, the central position showed different degrees of blueshift or

redshift, indicating that small molecules and proteins may form a complex. By contrast, *R*-nicotine had a greater influence on the 3D map of AChE than *S*-nicotine, suggesting that *R*-nicotine can exert a more significant influence on the conformation of AChE.

3.5.3 Synchronous fluorescence spectroscopy. Synchrotron fluorescence spectroscopy is a powerful tool for studying specific amino acids (tyrosine and tryptophan) in proteins, which avoids the effects of many other amino acids in the proteins.[49] When the wavelength difference between the excitation wavelength and the emission wavelength is $\Delta\lambda = 15$ nm and 60 nm, the spectral characteristics of tyrosine (Tyr) and tryptophan (Trp) are respectively indicated. After adding nicotine, *S*-nicotine had no obvious effect on the Tyr amino acid of AChE, and the peak position did not move, whereas *R*-nicotine caused a weak redshift of the maximum wavelength of the Tyr amino acid of the protein (Fig. 13). Both configurations of nicotine affected the Trp amino acid microenvironment of the AChE, given that there was a remarkable redshift in the maximum emission wavelength. The results showed that the amino acid microenvironment of AChE was changed by the binding of *S*/*R*-nicotine, and the effect of *R*-nicotine was greater than that of *S*-nicotine.

3.5.4 CD spectrum. The peptide bond contained in the protein has ultraviolet absorption in the 180–240 nm band, and the negative peak at about 208 nm (π–π^* transition) shows the α-helix structure of the protein.[50] Fig. 14(a) shows that the addition of *S*-nicotine increased the α-helical structure of AChE, but the total CD spectral properties (pattern) did not change. Thus, the addition of *S*-nicotine resulted in the increase of α-helical content of AChE, but the overall conformation did not undergo qualitative changes. By contrast, the CD spectrum of R-AChE changed significantly in both spectrum and peak shape [Fig. 14(b)], indicating that *R*-nicotine had an irreversible effect on the structure of AChE.

3.5.5 Effect of nicotine on the secondary structure of AChE in MD simulation. Fig. 15 shows the protein secondary structure (helix, sheet; turn, coil) content in the simulation process. The coil content accounted for the largest proportion, about 35.5% in the three systems. The addition of *S*-nicotine increased the coil content of AChE, whereas the content of sheet and turn was slightly reduced. This observation was consistent with the results of CD analysis. In the R-AChE system, the content of coil and turn fluctuated greatly. Thus, *R*-nicotine had an obviously influence on the secondary structure of AChE, which may cause a more significant influence on the conformation and function of AChE. Because of the deviations between computer simulation and actual experiments, only qualitative analysis can be done here.

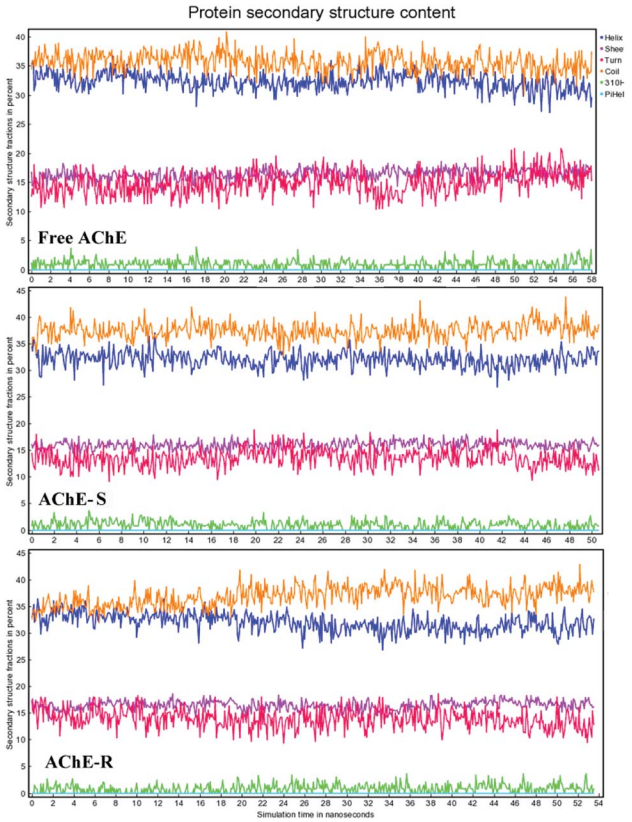

Fig. 15 Changes in the secondary structure content of the three systems of proteins during MD calculation. Line yellow: coil; blue: helix; purple:sheet; magenta: turn.

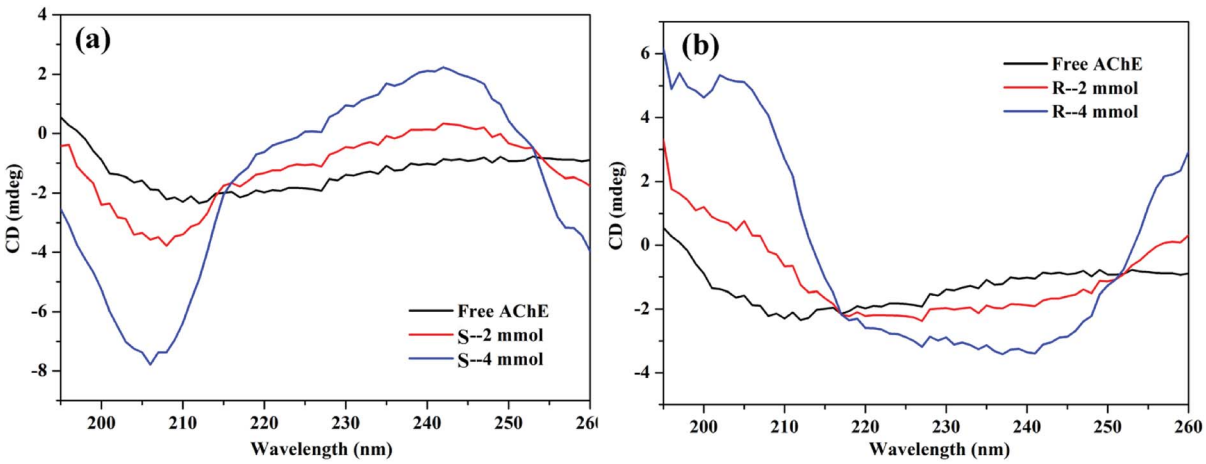

Fig. 14 Circular dichroism spectrum of the (a) AChE-*S*-nicotine and (b) AChE-*R*-nicotine systems at 298 K.

4. Conclusion

In this study, the interaction mode between *S*/*R*-nicotine and AChE was explored by experiments and computer simulation. Spectroscopic analysis showed that *S*/*R*-nicotine and AChE formed a ground-state complex with very weak binding strength with different driving forces, and there was only one major binding site. *R*-nicotine had a much greater effect on the conformation of AChE than *S*-nicotine, which may be due to the difference in the activity of *S*/*R*-nicotine. This finding was also verified by studying the effect of *S*/*R*-nicotine on enzyme activity of AChE. The results of computer simulation were consistent with the experimental results. MD simulation further confirmed that Tyr121 amino acid played an important role in the interaction, and the fluctuation of secondary structure content in the simulation process was also more obvious for *R*-nicotine than *S*-nicotine. In general, *R*-nicotine may have a more adverse effect on AChE than *S*-nicotine. The results provided reference for the commercialization and industrialization of nicotine products, and also presented a basis for analyzing the toxicological characteristics and biochemical behavior of nicotine.

Conflicts of interest

There are no conflicts to declare.

Acknowledgements

This work was supported by the tobacco corporation Key technology research on the quality stability of colloidal smokeless tobacco products from major science and technology special projects of China [110201601005(2016xx-05)], and the study on key technologies of tobacco in mouth based on comfort and oral health from Yunnan China tobacco industry company technology development program project (2018CP07).

References

1 J. N. Langley and W. L. Dickinson, *J. Physiol.*, 1890, **11**, 265–306.
2 J. D. Pilcher and T. Sollmann, *J. Pharmacol. Exp. Ther.*, 1915, **6**, 369–372.
3 E. Asmus and D. Papenfuss, *Fresenius' Z. Anal. Chem.*, 1962, **185**, 201–211.
4 M. A. Abbassy, M. E. Eldefrawi and A. T. Eldefrawi, *Pestic. Biochem. Physiol.*, 1983, **19**, 299–308.
5 B. Schafer, *Chem. Unserer Zeit*, 2008, **42**, 408–424.
6 A. Das, M. Dikshit and C. Nath, *Pharmacol., Biochem. Behav.*, 2005, **81**, 89–99.
7 J. Massoulie, L. Pezzementi, S. Bon, E. Krejci and F. M. Vallette, *Prog. Neurobiol.*, 1993, **41**, 31–91.
8 C. Scheffel, H. Thiermann and F. Worek, *Toxicol. Lett.*, 2015, **232**, 557–565.
9 H. Gnahn, F. Hefti, R. Heumann, M. E. Schwab and H. Thoenen, *Dev. Brain Res.*, 1983, **9**, 45–52.
10 M. Wang, G. Zhang, D. Zhang, D. Zhu and B. Z. Tang, *J. Mater. Chem.*, 2010, **20**, 1858–1867.
11 S. Wang, C. Wu, Z. Liu and H. You, *Toxicol. Lett.*, 2018, **287**, 42–48.
12 E. Ayranci and O. Duman, *Protein Pept. Lett.*, 2004, **11**, 331–337.
13 E. Ayranci and O. Duman, *Food Chem.*, 2004, **84**, 539–543.
14 M. Tanaka, Y. Asahi and S. Masuda, *J. Macromol. Sci., Part A: Pure Appl.Chem.*, 1995, **32**, 339–347.
15 B. K. Bozoglan, S. Tunc and O. Duman, *J. Lumin.*, 2014, **155**, 198–204.
16 J. H. Tang, F. Luan and X. G. Chen, *Bioorg. Med. Chem.*, 2006, **14**, 3210–3217.
17 S. Tunc, A. Cetinkaya and O. Duman, *J. Photochem. Photobiol., B*, 2013, **120**, 59–65.
18 S. Tunc, O. Duman and B. K. Bozoglan, *J. Lumin.*, 2013, **140**, 87–94.
19 S. Tunc, O. Duman, I. Soylu and B. K. Bozoglan, *J. Lumin.*, 2014, **151**, 22–28.
20 S. Tunc, O. Duman, I. Soylu and B. K. Bozoglan, *J. Hazard. Mater.*, 2014, **273**, 36–43.
21 O. Duman, S. Tunc and B. K. Bozoglan, *J. Fluoresc.*, 2013, **23**, 659–669.
22 M. Rarey, B. Kramer, T. Lengauer and G. Klebe, *J. Mol. Biol.*, 1996, **261**, 470–489.
23 E. Krieger and G. Vriend, *Bioinformatics*, 2014, **30**, 2981–2982.
24 J. Park, J. J. McDonald, R. C. Petter and K. N. Houk, *J. Chem. Theory Comput.*, 2016, **12**, 2066–2078.
25 A. Jakalian, D. B. Jack and C. I. Bayly, *J. Comput. Chem.*, 2002, **23**, 1623–1641.
26 P. L. T, M. Mondal, K. Ramadas and S. Natarajan, *Spectrochim. Acta, Part A*, 2017, **183**, 90–102.
27 N. Gan, Q. Sun, P. Tang, D. Wu, T. Xie, Y. Zhang and H. Li, *Spectrochim. Acta, Part A*, 2018, **206**, 126–134.
28 M. Pathak, D. Sharma, N. Sharma and M. Sharma, *J. Mol. Struct.*, 2018, **1166**, 183–189.
29 G. G. Ariga, P. N. Naik, S. A. Chimatadar and S. T. Nandibewoor, *J. Mol. Struct.*, 2017, **1137**, 485–494.
30 D. Wu, D. Liu, Y. Zhang, Z. Zhang and H. Li, *Eur. J. Med. Chem.*, 2018, **146**, 245–250.
31 E. T.-L. L. Karami and A. A. Saboury, *Phys. Chem. Res.*, 2017, **5**, 483–496.
32 H. Dvir, I. Silman, M. Harel, T. L. Rosenberry and J. L. Sussman, *Chem.-Biol. Interact.*, 2010, **187**, 10–22.
33 M. Harel, G. Kryger, T. L. Rosenberry, W. D. Mallender, T. Lewis, R. J. Fletcher, J. M. Guss, I. Silman and J. L. Sussman, *Protein Sci.*, 2000, **9**, 1063–1072.
34 G. Amitai, A. Shemesh, E. Sitbon, M. Shklar, D. Netanely, I. Venger and S. Pietrokovski, *J. Mol. Biol.*, 2004, **344**, 1135–1146.
35 Q. Wang, X. Ma, J. He, Y. Li and H. Li, *RSC Adv.*, 2015, **5**, 44696–44704.
36 D. P. Yeggoni, M. Gokara, D. M. Manidhar, A. Rachamallu, S. Nakka, C. S. Reddy and R. Subramanyam, *Mol. Pharmaceutics*, 2014, **11**, 1117–1131.
37 M. Raza, Y. Wei, Y. Jiang, A. Ahmad, S. Raza, S. Ullah, Y. Han, Q. U. Khan and Q. Yuan, *New J. Chem.*, 2017, **41**, 8203–8213.

38 P. Mitra, U. Pal, N. Chandra Maiti, A. Ghosh, A. Bhunia and S. Basu, *RSC Adv.*, 2016, **6**, 53454–53468.
39 H. Yang, Y. Huang, J. Liu, P. Tang, Q. Sun, X. Xiong, B. Tang, J. He and H. Li, *Sci. Rep.*, 2017, **7**, 11126.
40 S. J. Wang, Y. L. Peng, C. G. Zhang, Q. P. Ma, X. X. Peng and L. L. Ren, *Bull. Korean Chem. Soc.*, 2017, **38**, 735–743.
41 E. Kaspchak, L. I. Mafra and M. R. Mafra, *Food Chem.*, 2018, **252**, 1–8.
42 G. L. Ellman, K. D. Courtney, V. Andres and R. M. Featherstone, *Biochem. Pharmacol.*, 1961, **7**, 88–95.
43 S. Prasanth and C. Sudarsanakumar, *New J. Chem.*, 2017, **41**, 9521–9530.
44 Y. Zhan, J. Yang, L. Guo, F. Luo, B. Qiu, G. Hong and Z. Lin, *Sens. Actuators, B*, 2019, **279**, 61–68.
45 P. Barai, N. Raval, S. Acharya, A. Borisa, H. Bhatt and N. Acharya, *Behav. Brain Res.*, 2019, **356**, 18–40.
46 M. M. Yin, P. Dong, W. Q. Chen, S. P. Xu, L. Y. Yang, F. L. Jiang and Y. Liu, *Langmuir*, 2017, **33**, 5108–5116.
47 S. Zhuang, H. Wang, K. Ding, J. Wang, L. Pan, Y. Lu, Q. Liu and C. Zhang, *Chemosphere*, 2016, **144**, 1050–1059.
48 Q. Wang, Q. Sun, P. Tang, B. Tang, J. He, X. Ma and H. Li, *RSC Adv.*, 2015, **5**, 81696–81706.
49 V. Sinisi, C. Forzato, N. Cefarin, L. Navarini and F. Berti, *Food Chem.*, 2015, **168**, 332–340.
50 N. Gan, Q. Sun, M. Zhang, P. Tang, L. Zhao, T. Xie, Y. Zhang and H. Li, *J. Biomol. Struct. Dyn.*, 2018, DOI: 10.1080/07391102.2018.1502686.